**Shi-Chang Du**[1]
State Key Lab of Mechanical System and Vibration;
Department of Industrial Engineering and Management,
School of Mechanical Engineering,
Shanghai Jiaotong University,
Shanghai 200240, China
e-mail: lovbin@sjtu.edu.cn

**Tao Liu**
Department of Industrial Engineering and Management,
School of Mechanical Engineering,
Shanghai Jiaotong University,
Shanghai 200240, China
e-mail: l_yz2007@163.com

**De-Lin Huang**
Department of Industrial Engineering and Management,
School of Mechanical Engineering,
Shanghai Jiaotong University,
Shanghai 200240, China
e-mail: cjwanan@sjtu.edu.cn

**Gui-Long Li**
Department of Industrial Engineering and Management,
School of Mechanical Engineering,
Shanghai Jiaotong University,
Shanghai 200240, China
e-mail: lgllg68629315@qq.com

# An Optimal Ensemble Empirical Mode Decomposition Method for Vibration Signal Decomposition

*The vibration signal decomposition is a critical step in the assessment of machine health condition. Though ensemble empirical mode decomposition (EEMD) method outperforms fast Fourier transform (FFT), wavelet transform, and empirical mode decomposition (EMD) on nonstationary signal decomposition, there exists a mode mixing problem if the two critical parameters (i.e., the amplitude of added white noise and the number of ensemble trials) are not selected appropriately. A novel EEMD method with optimized two parameters is proposed to solve the mode mixing problem in vibration signal decomposition in this paper. In the proposed optimal EEMD, the initial values of the two critical parameters are selected based on an adaptive algorithm. Then, a multimode search algorithm is explored to optimize the critical two parameters by its good performance in global and local search. The performances of the proposed method are demonstrated by means of a simulated signal, two bearing vibration signals, and a vibration signal in a milling process. The results show that compared with the traditional EEMD method and other improved EEMD method, the proposed optimal EEMD method automatically obtains the appropriate parameters of EEMD and achieves higher decomposition accuracy and faster computational efficiency.* [DOI: 10.1115/1.4035480]

*Keywords: vibration signal decomposition, ensemble empirical mode decomposition, multimode search, mode mixing*

## 1 Introduction

Vibration signals carrying a lot of information about the mechanical equipment health condition are frequently applied to monitor the machine health condition. The vibration signal decomposition is a critical step in machine health monitoring and fault diagnosis [1–3]. The methods to decompose vibration sensor signal mainly include FFT, wavelet transform, and EMD [4]. Among these methods, the FFT is one of the most widely used and well-established methods. However, there are some crucial restrictions on the use of Fourier transform. On the one hand, the FFT is a typical linear and stationary transform, which is not suitable for nonstationary signal analysis. On the other hand, it is suitable for global signal analysis instead of local signal analysis. Unfortunately, the vibration signals to be analyzed are often nonstationary and nonlinear especially under time-varying operational conditions. Hence, the FFT cannot fully fulfill the requirements of health monitoring and fault diagnosis. Recently, wavelet transform has become one of the most powerful signal processing tools on nonstationary signal decomposition [5–11]. Detailed descriptions of the existing research on application of the wavelet transform in machine condition monitoring and fault diagnostics are reviewed in Ref. [12].

In 1998, Huang et al. introduced the EMD method for analyzing data from nonstationary and nonlinear processes, which is based on instantaneous frequency [13–17]. The major breakthrough of the EMD is that the basis functions are derived from the signal itself, hence, the analysis is adaptive. The EMD method is very suitable for nonlinear and nonstationary signal, which has been demonstrated to be an effective sensor signal analysis method [18,19]. However, the primary drawback of the original EMD is mode mixing caused by intermittency of the driving mechanisms [20,21]. Mode mixing is defined as a single intrinsic mode function (IMF) consisting of signals of widely disparate scales, or a signal of a similar scale residing in different IMF components. Mode mixing is often a consequence of abnormal events including the intermittency signal, the pulse interference, and the noise. The presence of abnormal events causes the abnormal distribution of the extreme points of the envelope obtained by the cubic spline interpolation in the EMD sifting process, which leads to the fact that decomposition result is a mixture of the signal and abnormal events. An EMD-based enhanced signal decomposition approach that synthetizes the original information content into a minimal number of relevant modes via a data-driven and automated procedure is developed in Ref. [22]. To solve the mode mixing problem, EEMD, a substantial improvement of EMD, is developed by Wu and Huang [23]. EEMD is a new noise-assisted data analysis method, which utilizes full advantage of the statistical characteristics of white noise to decompose signal. Since the EEMD method has improved the decomposition accuracy, it has been quickly adopted in machine health condition monitoring and fault diagnosis [24–33].

The performance of EEMD severely depends on the selection of two important parameters: the amplitude of added white noise

[1]Corresponding author.

Contributed by the Technical Committee on Vibration and Sound of ASME for publication in the Journal of Vibration and Acoustics. Manuscript received August 24, 2016; final manuscript received November 29, 2016; published online March 16, 2017. Assoc. Editor: Mohammed Daqaq.

  

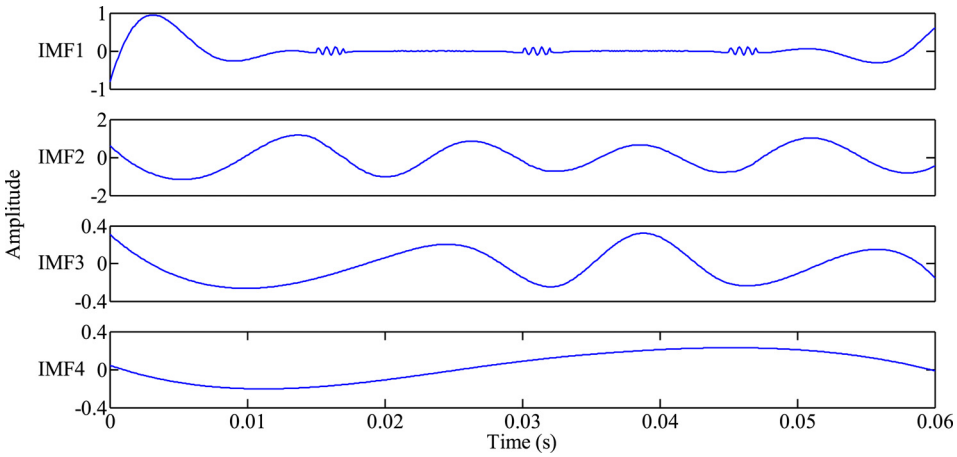


**Fig. 1 The decomposition results of EEMD including the intermittent signal**

and the number of ensemble trials. Although Wu and Huang [23] suggested that the amplitude of the added white noise is about 0.2 standard deviation of that of the original signal and a few hundreds of trials for ensemble will lead to a very good result, so far there are no specific methods to guide the EEMD parameter selection, which needs to be setup according to experience. By analyzing the effect of white noise on the decomposition in EMD, Chen et al. [34] established a criterion of the added white noise in EEMD. If the amplitude of the added noise is too small with respect to the original signal, a considerable elimination of mode mixing cannot be achieved. On the contrary, if the amplitude of the added noise is too large, it will create some redundant IMF components that lead to misinterpretation of the analysis result. Although an infinite number of ensemble trials is needed to completely cancel out the effect of the added white noise, too many trials would increase the computational cost [35]. By virtue of the inappropriate amplitude of added white noise for EEMD, nonideal results would occur. For example, a signal including an intermittent signal is decomposed by the traditional EEMD with the results shown in Fig. 1. IMF1 contains intermittent high-frequency signal and some of the low-frequency sinusoidal signal, which should appear in IMF2. It is clear that the problem of mode mixing appears among different IMFs. The frequency mixing has an obvious negative effect on the subsequent decomposition. IMF2 and IMF3 have a similar frequency of the waveform, but reside in different IMF components. So the intermittence not only causes serious aliasing in the time-frequency distribution but also makes the physical meaning of individual IMF unclear.

The main contribution of this paper is that a novel optimal EEMD method based on an adaptive algorithm and a multimode search algorithm is proposed to solve the mode mixing problem in vibration signal decomposition. Subsequently, the performances of the proposed method are demonstrated by means of a simulated signal, two bearing vibration signals, and a vibration signal in a milling process.

The rest of the paper is described as follows: In Sec. 2, brief introduction to EEMD is given. The optimal EEMD method is explored, and performance evaluation indices are presented in Sec. 3. A simulation experiment, two examples with bearing vibration signals, and a case study are presented in Secs. 4–6, respectively. The conclusion is given in Sec. 7.

## 2 Brief Introduction to Ensemble Empirical Mode Decomposition

The EEMD method utilizes important statistical characteristics of noise and the scale separation capability of the EMD method. The effects of the decomposition using the EEMD method are that the added white noise series cancel each other in the final mean of the corresponding IMFs; the mean IMFs stay within the natural dyadic filter windows, and thus it is significant to reduce the chance of mode mixing and preserve the dyadic property. The EEMD method can be briefly summarized as follows:

(1) Set the number of ensemble trials $N$ and the amplitude of the added white noise $\alpha$.
(2) Add random Gauss white noise with zero-mean to the original analyzed signal for $N$ times. The added amplitude standard deviation is constant

$$x_i(t) = x_o(t) + n_i(t) \tag{1}$$

where $x_o(t)$ is the original signal, $x_i(t)$ is the signal with the $i$th added white noise, and $n_i(t)$ is the $i$th added white noise ($i = 1, 2, ...N$).
(3) Decompose $x_i(t)$ by EMD to get the respective IMFs denoted $c_{ij}(t)$ and a residue of data denoted $r_i(t)$. $c_{ij}(t)$ denotes the $j$th IMF of decomposition of the $i$th added white noise to signal.
(4) If $i < N$, go to step (2) with $i = i + 1$; else go to the next step.
(5) Utilize the principle of uncorrelated random sequence statistics zero-mean, and calculate the above corresponding IMFs by an ensemble average way to get the final IMFs as the final results of EEMD method

$$c_j(t) = \frac{1}{N}\sum_{i=1}^{N} c_{ij}(t) \tag{2}$$

where $c_j(t)$ expresses the $j$th IMF component derived by EEMD.

According to Wu and Huang [23], the decomposition error $e$ is the final standard deviation of error, which is defined as the difference between the input signal and the corresponding IMFs, calculated by the following equation:

$$e = \sqrt{\frac{1}{T}\sum_{t=0}^{T}\left(\bar{X} - (x_o(t) - x_r(t))\right)^2} \tag{3}$$

where $x_r(t)$ is the reconstructed signal via the corresponding IMFs and the final residue decomposed by EEMD (Eq. (4)), $\bar{X}$ is the mean value of error (Eq. (5)), and $T$ is the total length of the original signal

$$x_r(t) = \sum_{j=1}^{n} c_j(t) + r_n(t) \tag{4}$$

$$\bar{X} = \frac{1}{T}\sum_{t=0}^{T}(x_o(t) - x_r(t)) \tag{5}$$

The relationship of the ensemble number $N$, the amplitude of the added white noise $\alpha$, and the decomposition error $e$ is given in the following equations:

$$e = \frac{\alpha}{\sqrt{N}} \tag{6a}$$

or

$$N = \left(\frac{\alpha}{e}\right)^2 \tag{6b}$$

## 3 The Proposed Method

The proposed method includes an adaptive algorithm and a multimode search algorithm. The adaptive algorithm is developed to automatically obtain the initial values of the added white noise amplitude and the ensemble number. The multimode search algorithm is explored to optimize the critical two parameters by its performance in global and local search. Thus, the two crucial parameters in EEMD are adaptively obtained. The optimal EEMD method is described in Fig. 2, and the algorithm is introduced in detail subsequently.

**3.1 Adaptive Algorithm.** The adaptive algorithm is described as follows:

Step 1: Input the original signal data.
Step 2: Calculate the amplitude standard deviation of the original signal denoted $\sigma_o$.
Step 3: Decompose the original signal by EMD method, obtain the first IMF regarded as high-frequency component information, and calculate the amplitude standard deviation of the first IMF denoted $\sigma_h$.
Step 4: Calculate the ratio coefficient $\varepsilon$ according to $\varepsilon = \sigma_h/\sigma_o$.
Step 5: Calculate the amplitude of the added white noise $\alpha_o$ according to $\alpha_o = \varepsilon/4$.
Step 6: Regard $\alpha_o$ as the initial value of the amplitude of the added white noise.

**3.2 Multimode Search Algorithm.** The adaptive algorithm is used to automatically obtain the initial values of the added white noise amplitude. In this section, the multimode search algorithm is developed to optimize the amplitude of the added white noise and the ensemble number.

In the multimode search algorithm, a varied step-length search strategy is designed so that the pattern direction is more approximated to efficient descent direction. The interpolation and nonmonotone technique are used in order to improve local search and global convergence. The multimode search algorithm alternates implementation of two searches from the initial point: axial search and pattern search. Axial search is an exploratory move designed to determine the new base point and the direction conducive to decrease the values of fitness function, and move in the direction of $m$-axis. Pattern search is a pattern move designed to utilize the information acquired in the exploratory moves, and accomplish the actual minimization of the function by moving in the conjunction direction of two adjacent base points.

Let $e_i = (0, \ldots, 0, 1, \ldots, 0)^{\mathrm{T}}$, $i = 1, 2, \ldots, m$ and $e_i$ denote unit vector and $m$ denote $m$ direction of axis. $x^k$ denotes the $k$th base point ($k$ is the search loop step number), and $y^i (i = 1, 2, \ldots, m)$ is used to indicate a starting point searching in the direction of the $i$th axis $e_i$. The multimode search algorithm is described as follows and its flowchart is shown in Fig. 3.

Step 1: The decomposition error (Eq. (3)) by EEMD method is set as the objective function $f(x)$, which is related to $\alpha$ and $N$.

Step 2: Select initial point $x^1$, initial step length $\theta > 0$ ($\theta$ is a $m$-dimensional vector rather than a numerical value), acceleration factor $\delta \geq 1$, increase rate of step length $\lambda > 1$, decrease rate of step length $\beta \in (0, 1)$, and accuracy requirement $\varepsilon \in (0.001, 0.01)$. Let $y^1 = x^1$, and $k = 1$.

Step 3: Start axial search mode. In every axial search, there are two search directions: one is along the positive direction $(+e_i)$ of the axis, and the other is the opposite $(-e_i)$, $i = 1, 2, \ldots, m$. Compare the values of $f(y^i + \theta(i) \times e_i) = f_{i1}$ (positive direction), $f(y^i - \theta(i) \times e_i) = f_{i2}$ (negative direction), and $f(y^i) = f_{i3}$.

Step 3.1: Positive direction axial search: If $f_{i1} < f_{i2} \leq f_{i3}$ or $f_{i1} < f_{i3} \leq f_{i2}$, let $y^{i+1} = y^i + \theta(i) \times e_i$ and $\theta(i) = \theta(i) \times \lambda$ (the search along the positive direction of the axis is effective).

Step 3.2: Negative direction axial search: If $f_{i2} < f_{i1} \leq f_{i3}$ or $f_{i2} < f_{i3} \leq f_{i1}$, let $y^{i+1} = y^i - \theta(i) \times e_i$ and $\theta = \theta \times \lambda$ (the search along the negative direction of the axis is effective); else let $y^{i+1} = y^i$ and search along another axis. The search should be along $m$-axes, and a value of $f(y^{m+1})$ is obtained.

Step 4: If $f(y^{m+1}) \geq f(x^k)$ (it means axial search mode fails and the process should be repeated until it succeeds), go to step 5. If $f(y^{m+1}) < f(x^k)$, go to step 6.

Step 5: Decrease step size, let $\theta = \theta \times \beta$, go to step 3.

Step 6: Start pattern search mode. Let $x^{k+1} = y^{m+1}$ and the direction of $(x^{k+1} - x^k)$ is probable to decrease the function value. Therefore, pattern search will be along that direction, which is $y^1 = x^{k+1} + \delta \times (x^{k+1} - x^k)$, let $k = k + 1$, go to step 3.

Step 7: If $f(y^{m+1}) < f(x^k)$ (it means pattern search mode succeeds), go to step 9. If $f(y^{m+1}) \geq f(x^k)$ (it means pattern search mode fails), go to step 8.

Step 8: Decrease step size, let $\theta = \theta \times \beta$ and $\delta = \delta \times \beta$, and back to step 3.

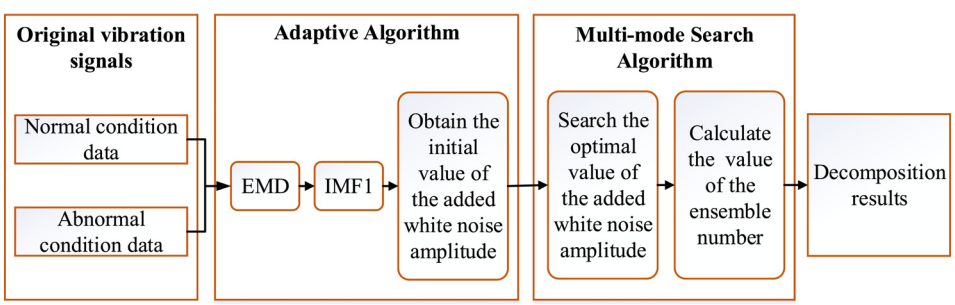


**Fig. 2 The framework of the optimal EEMD method**

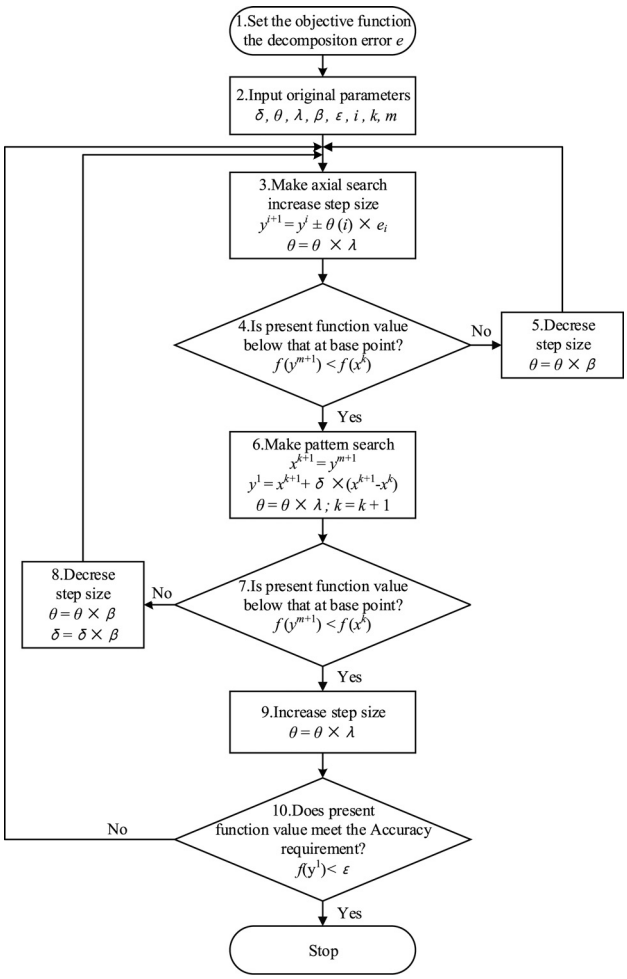


**Fig. 3 Flowchart of multimode search algorithm**

Step 9: Increase step size $\theta = \theta \times \lambda$, and go to step 10.

Step 10: If $f(y^1) < \varepsilon$, $i \in [1, m]$, then stop. If not, back to step 3.

An example of two-dimensional coordinate system is shown in Fig. 4. $e_i$ and $e_2$ are unit vectors, and $o$ is the origin of the coordinate. $x^1$ denotes the first base point of the first search loop. A loop process of axial and pattern search is explained elaborately as follows.

(1) Start axial search mode shown in Fig. 4(*a*). In the axial search of the $e_1$ axis, there are two search directions: the positive direction ($+e_1$) and the negative ($-e_1$). Let $y^1 = x^1$. Compare the values of $f(y^1 + \theta(1) \times e_1) = f_{11}$ (positive direction), $f(y^1 - \theta(1) \times e_1) = f_{12}$ (negative direction), and $f(y^1) = f_{13}$. If $f_{11} < f_{12} \le f_{13}$, search along the positive direction of the $e_1$ axis and obtain the new point $y^2$ of axial search. Similarly, if $f_{22} < f_{21} \le f_{23}$, search along the negative direction of the $e_2$ axis and obtain the new point $y^3$ of pattern search.

(2) Start pattern search mode shown in Fig. 4(*b*). Let $x^2 = y^3$. Compare the values of $f(x^1)$ and $f(y^3)$. If $f(y^3) < f(x^1)$, then start pattern search along the direction of $(x^2 - x^1)$, and obtain the new base point $y^1 = x^1 + \delta \times (x^2 - x^1)$.

(3) Start another axial and pattern search loop (step 6: let $k = k + 1$, go to step 3) shown in Fig. 4(*c*).

**3.3 Evaluation Indices and Competitor Methods.** Three widely used indices, i.e., decomposition error $e$ (Eq. (3)) [36,37], index of orthogonality (IO) of IMFs [38,39], and correlation coefficient [23,38,39], are applied to evaluate the performances of the proposed optimal EEMD method. The IO ($j \ne k, k = 1, 2, ..., n$) is shown in the following equation:

$$IO = \sum_{t=0}^{T} \left( \sum_{j}^{n+1} \sum_{k}^{n+1} c_j(t) c_k(t) / x^2(t) \right) \tag{7}$$

For two time series $X = \{x_i, i = 1, 2, ..., n\}$ and $Y = \{y_i, i = 1, 2, ..., n\}$, the correlation coefficient $\rho_{XY}$ of $X$ and $Y$ is calculated by

$$\rho_{XY} = \frac{\sum_{i=1}^{n} (x_i - \bar{x})(y_i - \bar{y})}{\sqrt{\sum_{i=1}^{n} (x_i - \bar{x})^2 \sum_{i=1}^{n} (y_i - \bar{y})^2}} \tag{8}$$

where $\bar{x} = \sum_{i=1}^{n} x_i / n$ and $\bar{y} = \sum_{i=1}^{n} y_i / n$. $\rho_{XY}$ is utilized to evaluate the correlation coefficient of the decomposed components with the original components.

A large value of decomposition error and a small correlation coefficient indicate a significant difference between the decomposed and the original components, and hence a poor performance of decomposition. The setting value of $e$ between 0.001 and 0.01 is usually acceptable. It should be noted that IO is a global evaluation criterion. The larger the IO value is, the worse the orthogonality of the IMFs is. The larger the correlation between the decomposed components with the original components is, the higher decomposition accuracy is. Ideally, if the IO value is zero, the IMFs are completely orthonormal.

Two competitor methods are used to compare the performance with the proposed optimal EEMD: the traditional EEMD [23] and the latest improved EEMD [34].

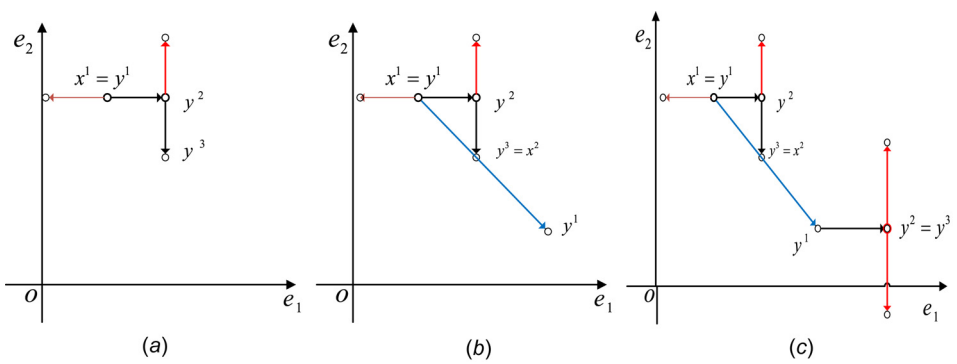


**Fig. 4 Axial search mode and pattern search mode in two-dimensional coordinate system**

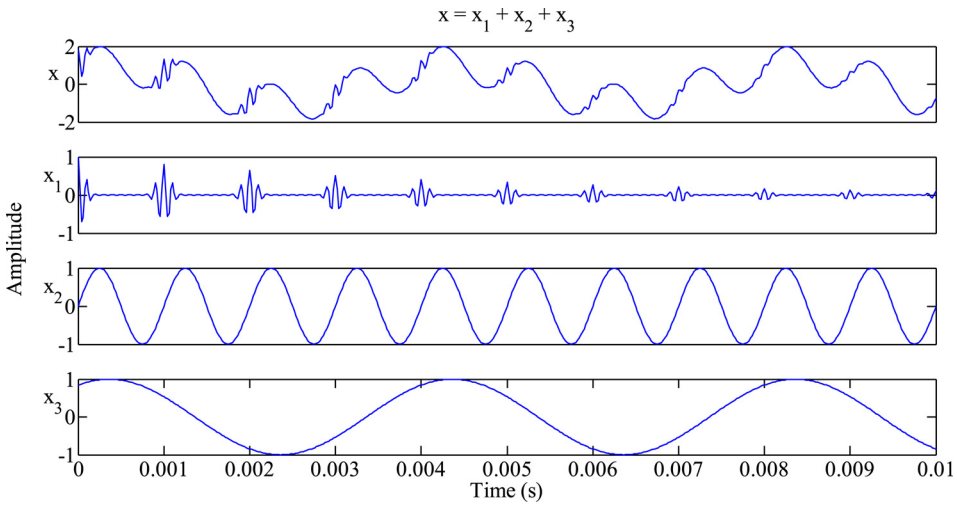


**Fig. 5 The simulated signal and its components**

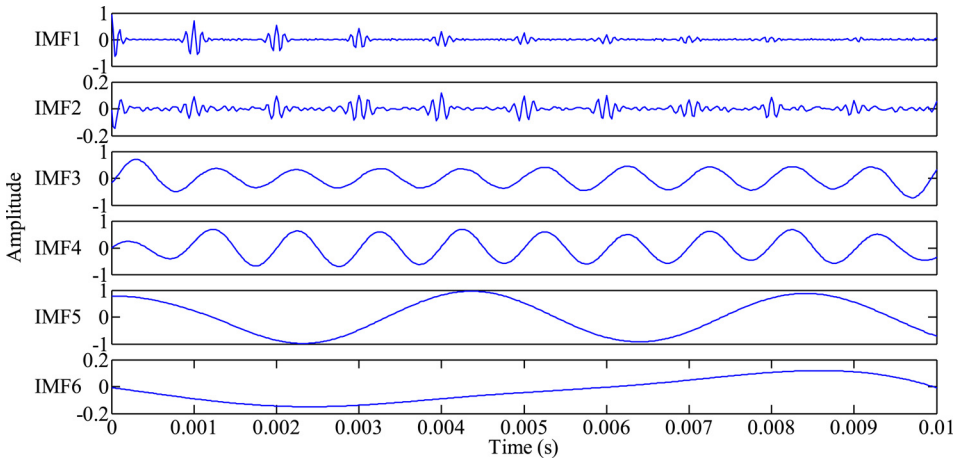


**Fig. 6 The decomposition results of the traditional EEMD**

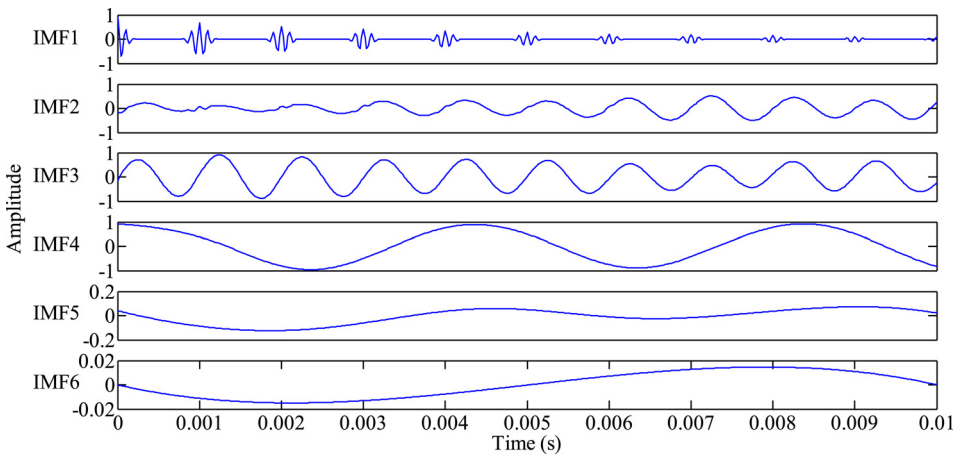


**Fig. 7 The decomposition results of the improved EEMD**

## 4 Simulation Experiment

**4.1 Simulation Results.** The simulated signal $x$ (Eq. (9)) shown in Fig. 5 contains a modulation Gaussian pulse wave and two sinusoid waves with same amplitudes, different initial phases, and frequencies. The main components of the simulated signal are given as follows:

$$x(t) = x_1(t) + x_2(t) + x_3(t) \tag{9}$$

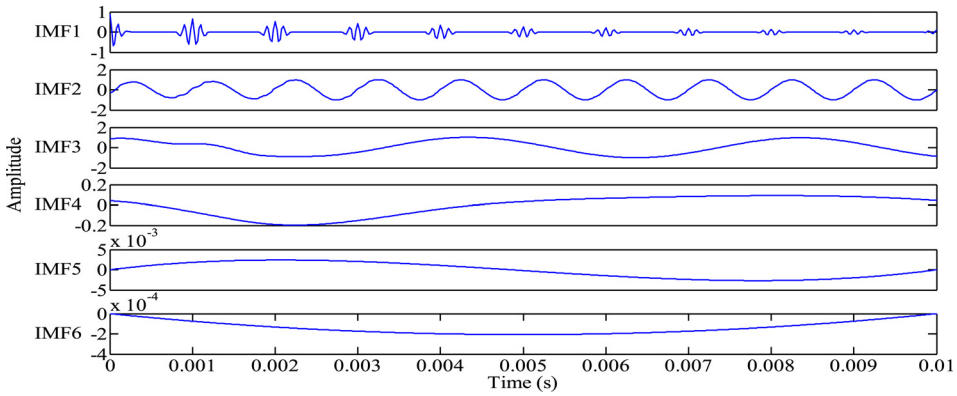


**Fig. 8 The decomposition results of the optimal EEMD**

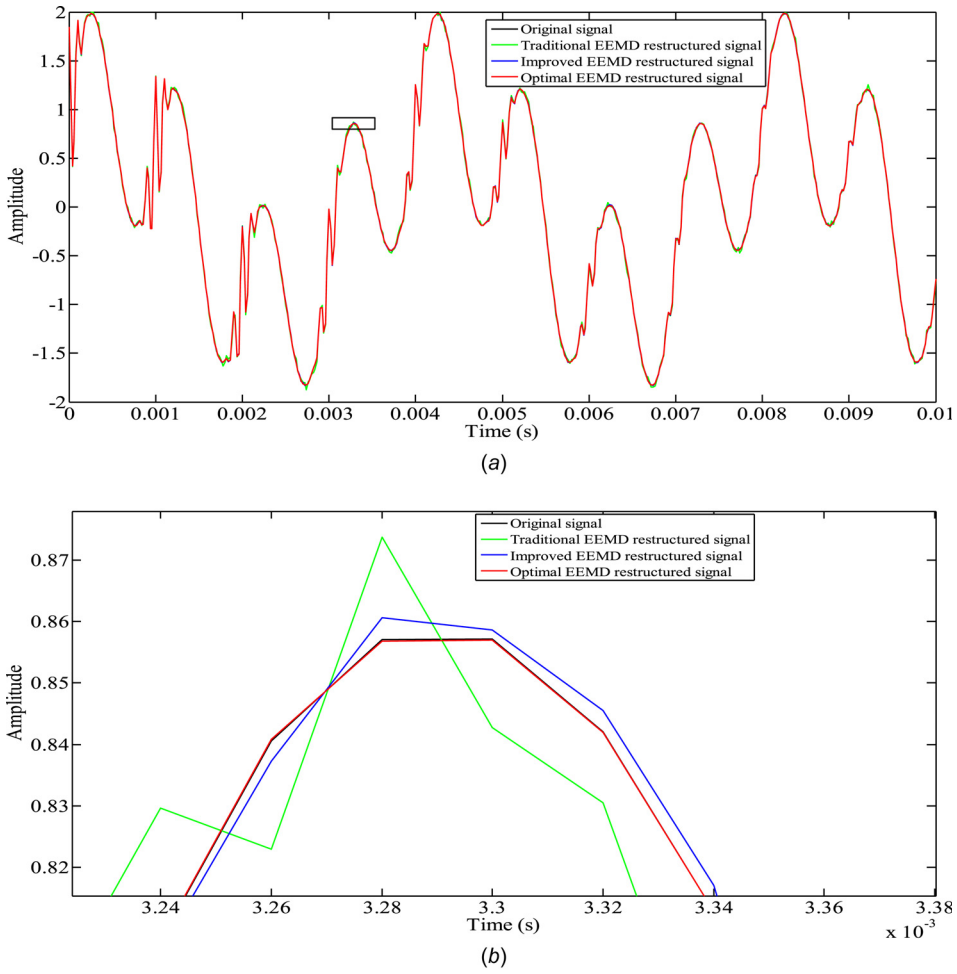


**Fig. 9 Comparison between reconstructed signal using three methods with the original signal**

$$x_2(t) = \sin(2\pi \times 1000t) \tag{10}$$

$$x_3(t) = \sin(2\pi \times 250t + 0.32\pi) \tag{11}$$

The modulation Gaussian pulse wave $x_1$ has the repetition rate of 1000 Hz, the pass band sawtooth width of 0.01 s, and the attenuation rate of 0.8. The two sinusoidal waves are $x_2$ (Eq. (10)) and $x_3$ (Eq. (11)). The sampling frequency is set as 50 kHz, and the sampling time is 0.01 s.

There are totally seven parameters: the ensemble number $N$, the amplitude of the added white noise $\alpha$, initial step length $\theta$, acceleration factor $\delta$, increase rate of step length $\lambda$, decrease rate of step length $\beta$, and accuracy requirement $\varepsilon$. These parameters are set as follows: (1) According to Ref. [23], in general, an ensemble number of a few hundred will lead to a very good result. In case study of Ref. [23], the ensemble number $N$ was set as 100, and the good result has been obtained. Therefore, the ensemble number $N$ for each case is set as 100. (2) In Ref. [23], the amplitude of the added white noise was suggested to be set as 0.2. According to the criterion of adding white noise in Ref. [34], the amplitude of the added white noise $\alpha$ was 0.0335. In this study, through the proposed adaptive algorithm and the multimode

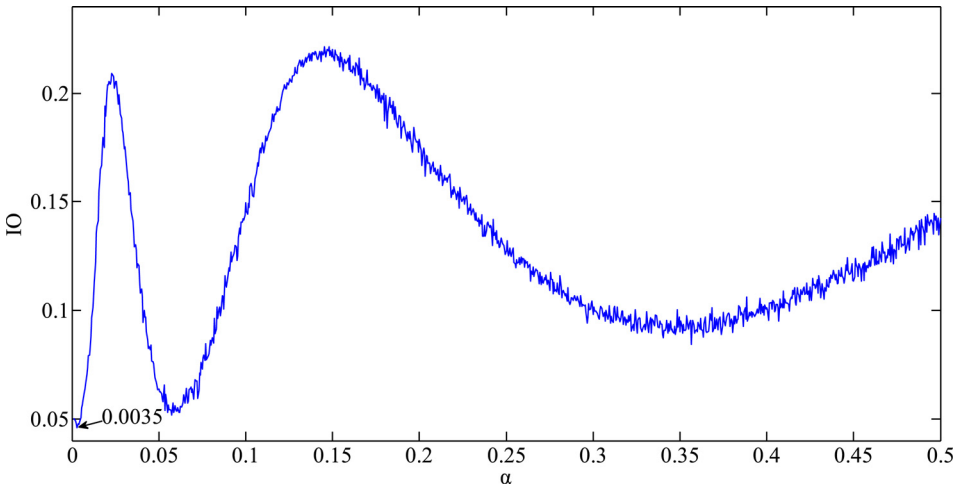


**Fig. 10 Relationship between the value of index of orthogonality IO and the amplitude ratio of white noise α**

search algorithm, the amplitude of the added white noise $\alpha$ was calculated and searched as 0.0035. (3) Initial step length $\theta > 0$, the value of initial step length was set as [0.01, 2]. The value of 0.01 is the variable quantity of the amplitude of the added white noise $\alpha$ in each step. The value of two is the variable quantity of the ensemble number of $N$ in each step. (4) According to Ref. [40], acceleration factor $\delta \geq 1$, in this study the value of acceleration factor $\delta$ was set as 1. (5) Increase rate of step length $\lambda \geq 2$. Because increase step size, $\theta = \theta \times \lambda$. To ensure the ensemble number $N$ in the initial step length $\theta$ is integer, the value of increase rate of step length was chosen as the least integer 2. (6) Decrease rate of step length $\beta < 1$. Because decrease step size, $\theta = \theta \times \beta$. To ensure the ensemble number $N$ in the initial step length $\theta$ is integer, the value of decrease rate of step length was chosen as the decimal 0.5. (7) Accuracy requirement $\varepsilon$ is the minimum allowable decomposition error. The value of $e$ was set as 0.001, this value is far lower than 0.1 which is acceptable in Ref. [23]. In summary, the parameters are in the maximum range, and the optimal results through them can be obtained. The setting of the initial parameters is the same as in the following examples.

The decomposition results of the traditional EEMD [23], the improved EEMD [34], and the optimal EEMD are shown in Figs. 6–8, respectively. Figure 9(*a*) shows the reconstructed signals using three methods and the original signals, and Fig. 9(*b*) shows a part of the result of Fig. 9(*a*) in range of 3.20 ms to 3.38 ms of time, which is chosen arbitrarily.

From these figures, some findings can be obtained.

(1) From Fig. 6, two sets of IMF components (IMF1 and IMF2, IMF3 and IMF4) have a similar scale and mutual influence. The correlation coefficients of IMF1 and IMF2, IMF3 and IMF4 are 0.5267 and 0.87. The three components cannot be separated into different IMFs, and mode mixing problem occurs.
(2) From Fig. 7, the correlation coefficients of IMF2 and IMF3, IMF4 and IMF5 are 0.8473 and 0.5152, respectively, which implies that the amplitude ratio of added white noise is relatively large and the redundant components IMF2 and IMF5 are generated.
(3) From Fig. 8, IMF1, IMF2, and IMF3 represent $x_1$, $x_2$, and $x_3$, respectively. There is no redundant component compared with Fig. 7.
(4) From Fig. 9(*a*), it can be seen that the curves are very difficult to distinguish the differences between the reconstructed signals using three methods and the original signals. Figure 9(*b*) illustrates the difference between the reconstructed signal using the traditional EEMD and the original signal is largest, the difference between the reconstructed signal using the improved EEMD and the original signal is in the middle, and the difference between the reconstructed signal using the optimal EEMD and the original signal is smallest. Therefore, the optimal EEMD method can effectively eliminate mode mixing and separate signals of different scales compared with the traditional EEMD [23] and the improved EEMD [34].

**4.2 Evaluation and Discussion.** In order to further validate the effectiveness of the proposed method, four aspects are discussed. In order to ensure the accuracy of the experiment data, the experiment was conducted for each group of the same $\alpha$ and $N$ with 100 times, and the mean is regarded as the final result.

(1) $N = 100$, $\alpha = 0.001, 0.0015, \ldots, 0.5$ are chosen to obtain the relationship between the IO value and the amplitude ratio of white noise $\alpha$, as shown in Fig. 10.
(2) The decomposition error and index of orthogonality are compared with the same $N$ ($N = 10, 15, \ldots, 95, 100$) value, as shown in Tables 1 and 2.
(3) The correlation coefficients between the decomposed components and the real components are compared with the same $N$ ($N = 100$) value, as shown in Table 3.
(4) The computational efficiency and decomposition accuracy are calculated and compared with the same decomposition error ($e = 0.01$) for different $\alpha$, as shown in Table 4.

The main conclusions are included as follows:

(1) It can be seen from Fig. 10 that the IO value is minimum when $\alpha = 0.0035$ in the range of [0.001, 0.5], i.e., at this point the decomposition accuracy is the highest.
(2) Table 1 shows that the decomposition error of the improved EEMD is approximately equal to one-sixth of the one of the traditional EEMD, and the decomposition error of the optimal EEMD is approximately equal to one-tenth of the one of the improved EEMD. The results shown in Table 1 also suggest that for the fixed $\alpha$ value, accordingly, the $e$ value decreases when the $N$ value increases.
(3) In Table 2, for the same $N$ value, the mean IO values of the traditional EEMD, the improved EEMD, and the optimal EEMD are 0.1698, 0.1471, and 0.0473, respectively. That is to say, the IO values of IMFs obtained by the traditional EEMD and the improved EEMD are larger, and the decomposition accuracies are lower. The IO of IMFs derived by the optimal EEMD is better, and the decomposition accuracy is higher. According to the above results, the influence

**Table 1 Comparison of decomposition error with the same *N* value**

| Ensemble number | Traditional EEMD [23] decomposition error ($e1$) | Improved EEMD [34] decomposition error ($e2$) | Optimal EEMD decomposition error ($e3$) | $e2/e1$ | $e3/e2$ |
|---|---|---|---|---|---|
| 10 | 0.0639 | 0.0111 | 0.00113 | 0.1733 | 0.1021 |
| 15 | 0.0534 | 0.0089 | 0.00095 | 0.1661 | 0.1069 |
| 20 | 0.0476 | 0.0077 | 0.00081 | 0.1620 | 0.1051 |
| 25 | 0.0417 | 0.0070 | 0.00072 | 0.1685 | 0.1026 |
| 30 | 0.0378 | 0.0063 | 0.00066 | 0.1661 | 0.1051 |
| 35 | 0.0349 | 0.0058 | 0.00062 | 0.1673 | 0.1065 |
| 40 | 0.0325 | 0.0055 | 0.00057 | 0.1704 | 0.1025 |
| 45 | 0.0306 | 0.0052 | 0.00054 | 0.1697 | 0.1034 |
| 50 | 0.0293 | 0.0049 | 0.00050 | 0.1665 | 0.1034 |
| 55 | 0.0280 | 0.0047 | 0.00049 | 0.1663 | 0.1045 |
| 60 | 0.0269 | 0.0044 | 0.00047 | 0.1635 | 0.1059 |
| 65 | 0.0260 | 0.0043 | 0.00044 | 0.1640 | 0.1038 |
| 70 | 0.0249 | 0.0041 | 0.00044 | 0.1655 | 0.1056 |
| 75 | 0.0239 | 0.0039 | 0.00043 | 0.1647 | 0.1083 |
| 80 | 0.0230 | 0.0039 | 0.00041 | 0.1675 | 0.1058 |
| 85 | 0.0224 | 0.0038 | 0.00039 | 0.1690 | 0.1041 |
| 90 | 0.0216 | 0.0036 | 0.00038 | 0.1665 | 0.1067 |
| 95 | 0.0211 | 0.0036 | 0.00036 | 0.1702 | 0.1016 |
| 100 | 0.0209 | 0.0035 | 0.00035 | 0.1658 | 0.1023 |
| | | Mean | | 0.1670 | 0.1045 |
| | | 1/mean | | 5.9882 | 9.5662 |

**Table 2 Comparison of index of orthogonality with the same *N* value**

| Ensemble number | Traditional EEMD [23] | Improved EEMD [34] | Optimal EEMD |
|---|---|---|---|
| 10 | 0.1388 | 0.1334 | 0.0385 |
| 15 | 0.1656 | 0.1245 | 0.0453 |
| 20 | 0.1561 | 0.1326 | 0.0468 |
| 25 | 0.1719 | 0.1476 | 0.0464 |
| 30 | 0.1746 | 0.1421 | 0.0509 |
| 35 | 0.1766 | 0.1518 | 0.0499 |
| 40 | 0.1696 | 0.1535 | 0.0463 |
| 45 | 0.1685 | 0.1541 | 0.0465 |
| 50 | 0.1721 | 0.1454 | 0.0490 |
| 55 | 0.1732 | 0.1497 | 0.0466 |
| 60 | 0.1742 | 0.1542 | 0.0475 |
| 65 | 0.1740 | 0.1508 | 0.0483 |
| 70 | 0.1759 | 0.1484 | 0.0485 |
| 75 | 0.1749 | 0.1478 | 0.0483 |
| 80 | 0.1697 | 0.1527 | 0.0464 |
| 85 | 0.1684 | 0.1502 | 0.0467 |
| 90 | 0.1729 | 0.1506 | 0.0479 |
| 95 | 0.1744 | 0.1523 | 0.0496 |
| 100 | 0.1743 | 0.1525 | 0.0486 |
| Mean | 0.1698 | 0.1471 | 0.0473 |

**Table 3 Comparison of correlation coefficient with the same *N* value**

| Comparative item | Traditional EEMD [23] | Improved EEMD [34] | Optimal EEMD |
|---|---|---|---|
| $x_1$ | 0.9733 | 0.9907 | 0.9915 |
| $x_2$ | 0.9680 | 0.9820 | 0.9948 |
| $x_3$ | 0.9894 | 0.9906 | 0.9920 |

**Table 4 Comparison of computational efficiency and decomposition accuracy with the same decomposition error**

| Comparative item | Traditional EEMD [23] | Improved EEMD [34] | Optimal EEMD |
|---|---|---|---|
| $\alpha$ | 0.2 | 0.0335 | 0.0035 |
| $N$ | 400 | 11 | 1 |
| Computational time (s) | 53.44 | 1.41 | 0.10 |
| IO | 0.1746 | 0.1334 | 0.0485 |

of the change of the $N$ value on IO can be neglected when $\alpha$ value is selected.

(4) The correlation coefficients between the decomposed components and the real components are given in Table 3. Compared to the traditional EEMD and the improved EEMD, the optimal EEMD has relatively larger correlation coefficients, i.e., it has less reconstruction error.

(5) Table 4 shows the IO values of the decomposed results and the computational time of these three methods. It is distinct that the decomposed results derived by the optimal EEMD have the smallest orthogonal coefficient. Moreover, the computational time of the optimal EEMD is much less than other two methods.

In summary, the results indicate that compared with the traditional EEMD and the improved EEMD, the optimal EEMD method has advantages in aspects of eliminating mode mixing,

**Table 5 Specification and characteristic frequency of the bearing (JEM SKF 6205-2RS)**

| Parameter | Value |
|---|---|
| Inside diameter | 25 mm |
| Outside diameter | 52 mm |
| Thickness | 15 mm |
| No. of balls, $N_b$ | 9 |
| Inner ring fault diameter | 0.1778 mm |
| Inner ring fault depth | 0.2794 mm |
| Shaft rotation speed, $f_z$ | 1796 rpm (29.93 Hz) |
| Sampling frequency | 12 kHz |
| Sample size | 10,000 |
| Inner ring defect frequency, $f_i$ | 162.1 Hz |
| Outer ring defect frequency, $f_o$ | 107.3 Hz |
| Cage train defect frequency, $f_c$ | 11.92 Hz |

**Table 6 Comparison of vibration signals' analysis from normal bearings' inner race**

| Comparative item | Traditional EEMD [23] | Improved EEMD [34] | Optimal EEMD |
|---|---|---|---|
| $\alpha$ | 0.2 | 0.1973 | 0.0082 |
| $N$ | 400 | 389 | 1 |
| Computational time (s) | 390.4 | 355.3 | 1 |
| IO | 0.1891 | 0.1889 | 0.0128 |

achieving higher decomposition accuracy, and saving computational time.

## 5 Examples With Bearing Vibration Signals

**5.1 Example 1: Bearing Inner Ring.** In this example, the bearing data set is obtained from Case Western Reserve University Bearing Data Center [41], which is the standard data set for analysis of vibration signals. The vibration signals are collected from normal and defective bearing inner ring. The tested bearings are JEM SKF 6205-2RS, and Table 5 shows the specification and characteristic frequency of the bearings.

*5.1.1 Vibration Signal Analysis of Normal Bearing.* For the vibration signals from normal bearing inner race, the amplitude of added white noise $\alpha$ of the traditional EEMD, the improved EEMD, and the optimal EEMD is 0.2, 0.1973, and 0.0082, respectively. The decomposition error is fixed as 0.01, and the $N$ values are 400, 389, and 76 accordingly. The computational time and the orthogonality values are shown in Table 6. The IO values obtained by the traditional EEMD and the improved EEMD are larger, the decomposition accuracies are lower, and mode mixing cannot be eliminated. However, the IO values obtained by applying the optimal EEMD are approximately equal to 1/14 of the two former values, which means that the decomposition accuracy is improved and mode mixing is reduced. It is clear that the computational time of the optimal EEMD is less than other two methods, and the calculation efficiency is improved.

Figure 11 is the decomposition result of vibration signals from normal bearing inner ring decomposed by the optimal EEMD, where $N$ for each case is set as 100. To extract the information more accurately, Hilbert–Huang transform (HHT) spectrum and FFT spectrum of IMFs obtained by the optimal EEMD are calculated. Figures 12 and 13 are the HHT spectrum and the FFT spectrum accordingly. From Fig. 11, it can be seen that IMF1 has a high-frequency periodic component. In Fig. 12, there is an interesting phenomenon that at the frequency of 1000 Hz, the energy

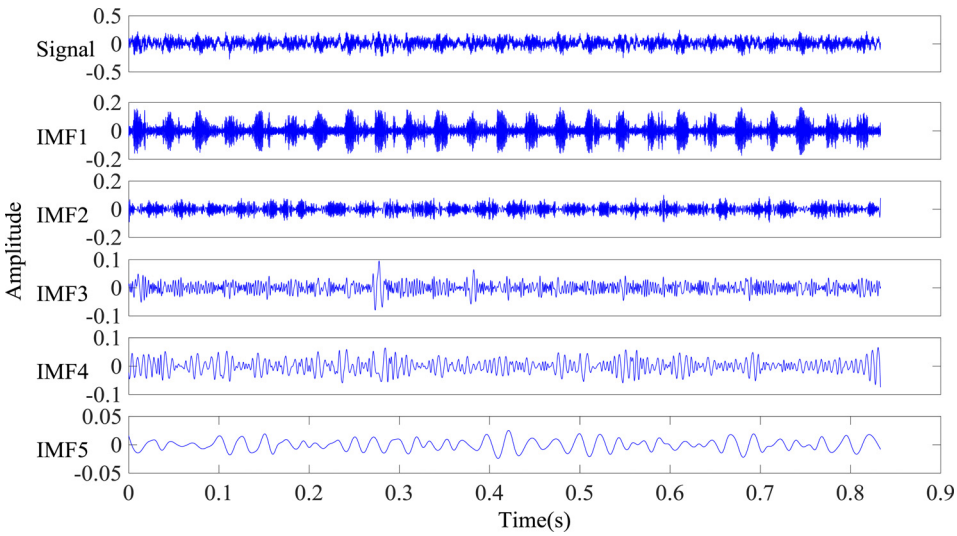


**Fig. 11 Result of vibration signals from normal bearings decomposed by the optimal EEMD**

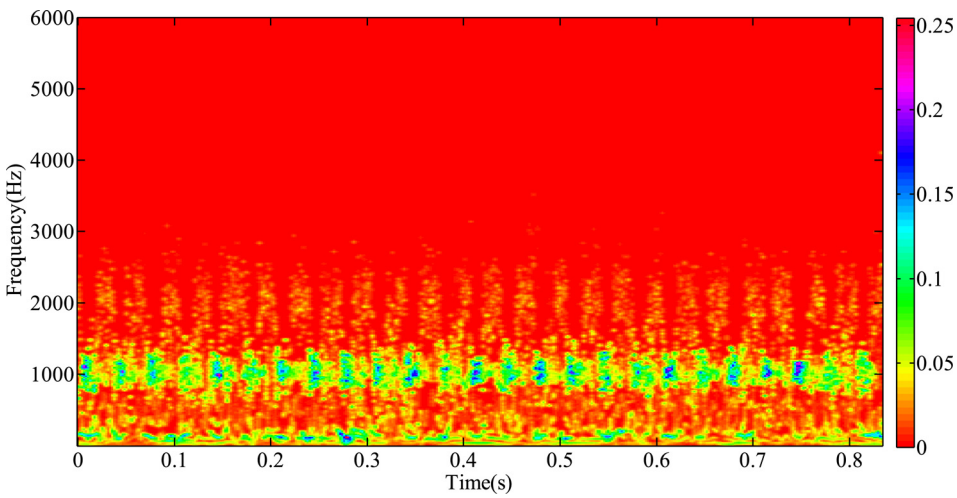


**Fig. 12 The HHT spectrum of normal bearing signals decomposed by the optimal EEMD**

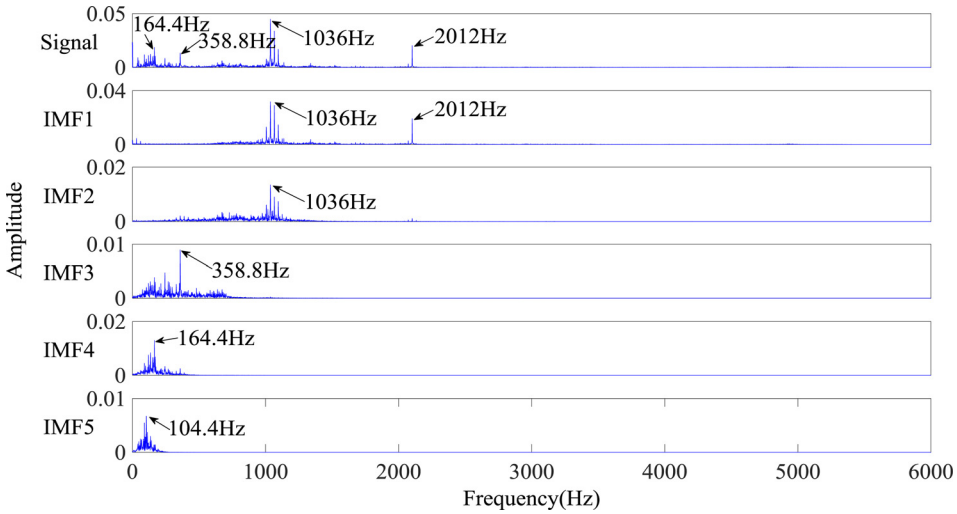


**Fig. 13 The frequency spectrum of normal bearing signals decomposed by the optimal EEMD**

**Table 7 Comparison of vibration signals' analysis from bearing inner race defect**

| Comparative item | Traditional EEMD [23] | Improved EEMD [34] | Optimal EEMD |
|---|---|---|---|
| $\alpha$ | 0.2 | 0.2375 | 0.0325 |
| $N$ | 400 | 564 | 11 |
| Computational time (s) | 431.7 | 610.2 | 12.2 |
| IO | 0.0102 | 0.0118 | 0.0006 |

density distribution is most concentrated. It can be seen from Fig. 13 that frequencies such as 358.8 Hz, 164.4 Hz, and 104.4 Hz in the FFT spectrum are clear.

*5.1.2 Vibration Signal Analysis of Defective Bearing*. For the vibration signal from detective bearing inner race, the amplitude of the added white noise $\alpha$ of the traditional EEMD, the improved EEMD, and the optimal EEMD is 0.2, 0.2375, and 0.0325, respectively. When the decomposition error is fixed as 0.01, the $N$ values are 400, 564, and 163 accordingly. Table 7 illustrates the computational time and the orthogonality values. The IO values obtained by the traditional EEMD and the improved EEMD are approximately equal to 1%, the decomposition accuracy is similar. In comparison, the IO value of the optimal EEMD is only 1/17 of the traditional EEMD's and 1/19 of the improved EEMD's. The results show that the decomposition accuracy is increased. It is clear that the computational time of the optimal EEMD is approximately equal to 1/35 of the traditional EEMD's and 1/50 of the improved EEMD's, and the computational efficiency is improved.

Figure 14 illustrates the decomposition results of bearing inner ring defect vibration signals decomposed by the optimal EEMD. Figures 15–17 are the HHT spectrum, the FFT spectrum, and the envelope spectrum, respectively. From the HHT spectrum and the FFT spectrum, it can be observed that every IMF component is decomposed nearly perfect by the optimal EEMD, and mode mixing is effectively reduced. It is known that 162.1 Hz is the theoretical fault frequency of bearing inner race, and 162 Hz is almost equal to the theoretical fault frequency. Meanwhile, 30 Hz is almost equal to the shaft rotation speed ($f_z = 29.93$ Hz) as shown in Table 5. In the envelope spectrum, the spectrum lines of the inner ring fault frequency ($f_i = 162$ Hz), twice inner ring fault frequency ($2f_i = 324$ Hz), four times of inner ring fault frequency ($4f_i = 648$ Hz), rotation frequency (30 Hz), and double frequency

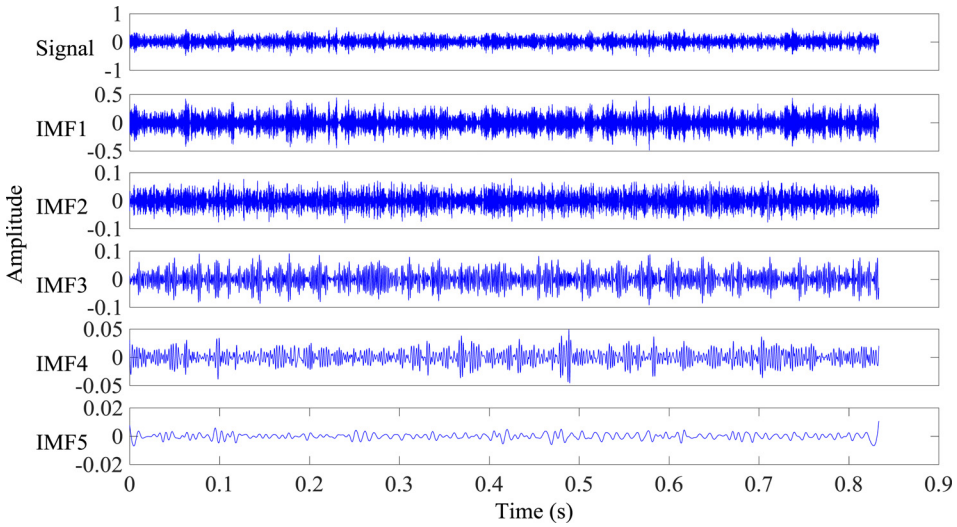


**Fig. 14 Results of vibration signals from defective bearing decomposed by the optimal EEMD**

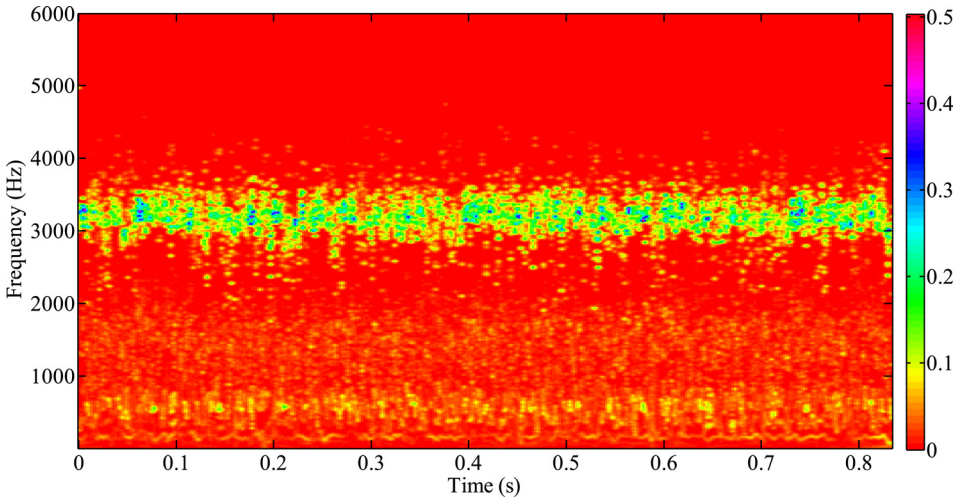


**Fig. 15 The HHT spectrum of defective bearing signals decomposed by the optimal EEMD**

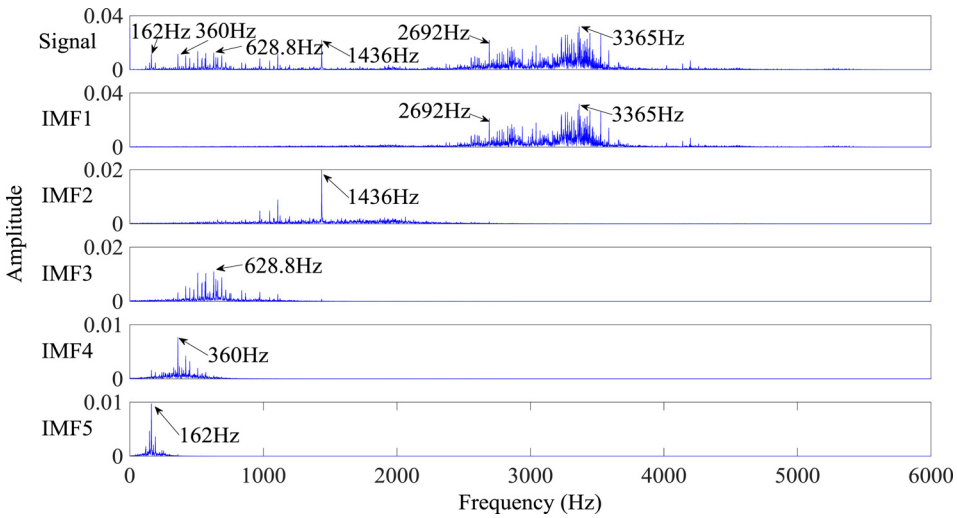


**Fig. 16 The frequency spectrum of defective bearing signals decomposed by the optimal EEMD**

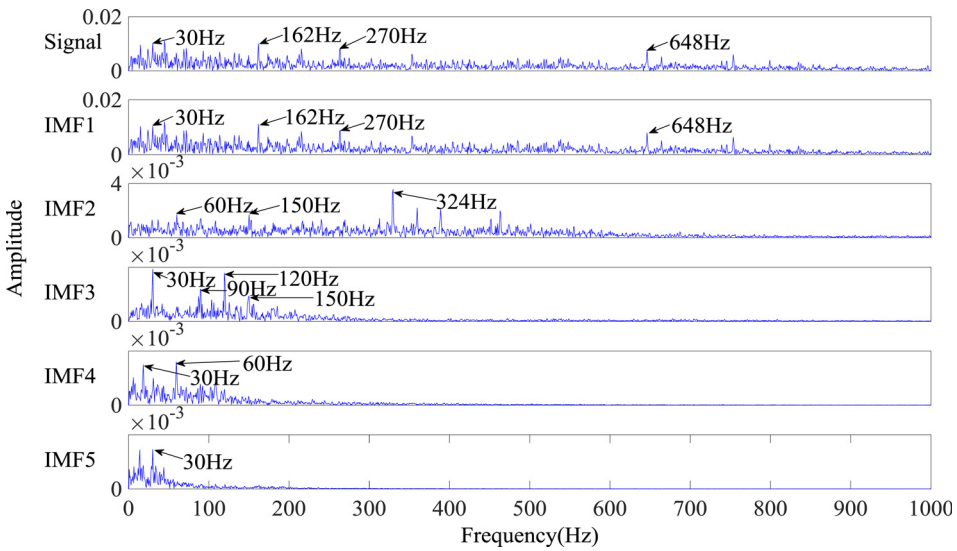


**Fig. 17 The envelope spectrum of defective bearing signals decomposed by the optimal EEMD**

**Table 8 Specification and characteristic frequency of the bearing**

| Parameter | Value |
|---|---|
| Pitch diameter | 71.5 mm |
| Roller diameter | 8.4 mm |
| No. of rollers, $N_b$ | 16 |
| Shaft rotation speed, $f_z$ | 2000 rpm (33.33 Hz) |
| Sampling frequency | 20 kHz |
| Sample size | 10,000 |
| Outer ring defect frequency | 236.40 Hz |
| Tapering contact angle | 15.17 deg |

**Table 9 Comparison of vibration signals' analysis from normal bearings' outer race**

| Comparative item | Traditional EEMD [23] | Improved EEMD [34] | Optimal EEMD |
|---|---|---|---|
| $\alpha$ | 0.2 | 0.1796 | 0.0196 |
| $N$ | 400 | 322 | 4 |
| Computational time (s) | 376.8 | 278.8 | 3.5 |
| IO | 0.0721 | 0.0673 | 0.0038 |

are very distinct. In the FFT spectrum, the high-frequency region with the center frequency of 3365 Hz has the sideband of the theoretical fault frequency of bearing inner race. In middle-frequency region and low-frequency region, the specific frequency components of 2692 Hz ($10 \times 9f_z$), 1436 Hz ($9f_i - f_z$), 628.8 Hz ($4f_i - f_z$), and 360 Hz ($2f_i + f_z$) are obviously double-frequency components of the shaft rotation speed, double-frequency components of inner ring defect frequency, and their sideband components. These results are consistent with the failure law of bearing inner race. Hence, the optimal EEMD can effectively decompose the vibration signals from the detective bearing inner ring.

**5.2 Example 2: Bearing Outer Ring.** In order to further validate the performance of the proposed method, another case is conducted. The data in this case are generated by the NSF I/UCR Center for Intelligent Maintenance Systems (IMS) with support from Rexnord Corp. [42]. The vibration signals are collected from normal and defective bearing outer ring. The model of the tested bearing is Rexnord ZA-2115 double row bearings, and the specification and characteristic frequency of the bearing are shown in Table 8.

*5.2.1 Vibration Signal Analysis of Normal Bearing.* For the vibration signals from normal bearing outer race, the amplitude of added white noise $\alpha$ of the traditional EEMD, the improved EEMD, and the optimal EEMD is 0.2, 0.1796, and 0.0196,

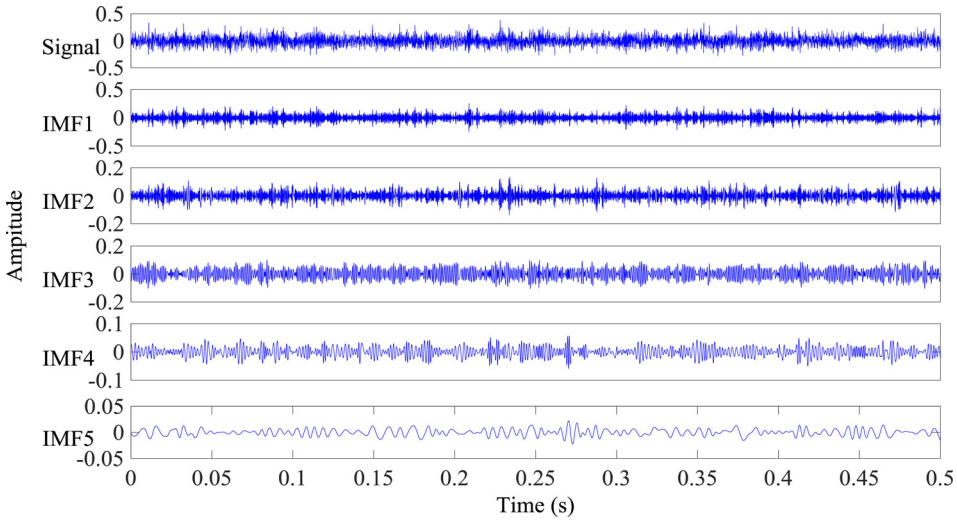


**Fig. 18 Result of vibration signal from normal bearings decomposed by the optimal EEMD**

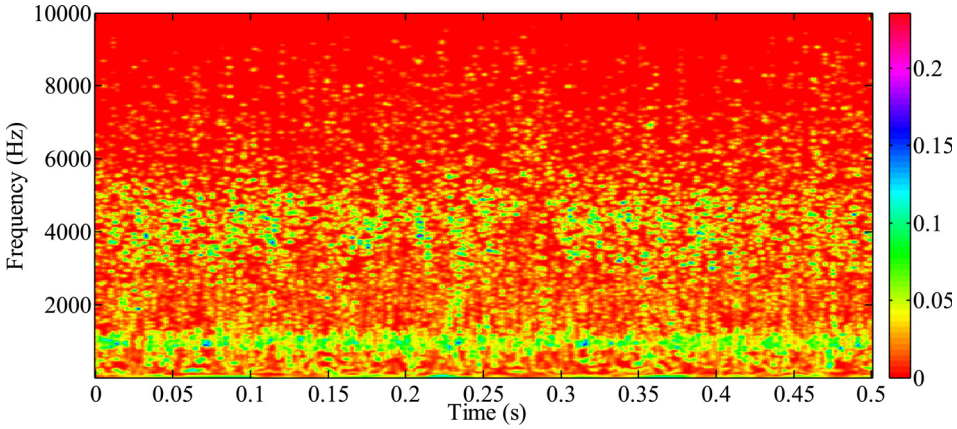


**Fig. 19 The HHT spectrum of normal bearing signals decomposed by the optimal EEMD**

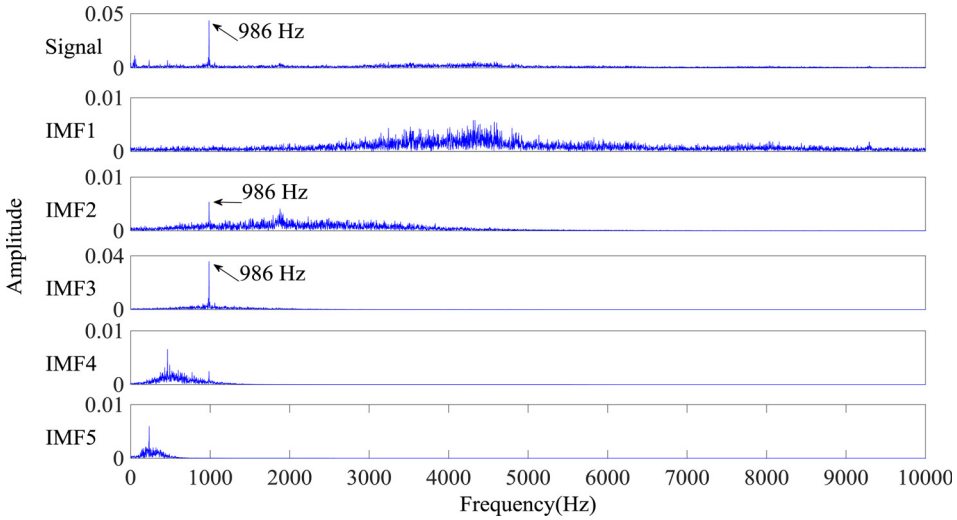


**Fig. 20 The frequency spectrum of normal bearing signals decomposed by the optimal EEMD**

**Table 10 Comparison of vibration signals' analysis from bearing outer race defect**

| Comparative item | Traditional EEMD [23] | Improved EEMD [34] | Optimal EEMD |
|---|---|---|---|
| $\alpha$ | 0.2 | 0.2062 | 0.0187 |
| $N$ | 400 | 425 | 4 |
| Computational time (s) | 425.9 | 523.5 | 6.0 |
| IO | 0.0445 | 0.0458 | 0.0162 |

respectively. When the decomposition error is set as 0.01, the $N$ values are 400, 322, and 4 accordingly. The computational time and the orthogonality value are shown in Table 9. The IO value of the traditional EEMD is quite close to the improved EEMD's. However, the IO value of the optimal EEMD is approximately equal to 1/18 of the two former's, which means that the decomposition accuracy is improved and the mode mixing is reduced. Obviously, the computational time of the optimal EEMD is less compared to the two former's, and the calculation efficiency also has certain improvement.

Figure 18 is the decomposition result of vibration signals from normal bearing outer ring decomposed by the optimal EEMD, where $N$ for each case is set as 100. Figures 19 and 20 are the HHT spectrum and the FFT spectrum, respectively. In Fig. 19, the energy density distribution is most concentrated near by the frequency of 1000 Hz. From Fig. 20, it can be seen that the frequency of 986 Hz is the dominant frequency. The result of Fig. 20 is consistent with the result of Fig. 19.

*5.2.2 Vibration Signal Analysis of Defective Bearing.* For the vibration signal from detective bearing outer race, the amplitude of added white noise $\alpha$ of the traditional EEMD, the improved EEMD, and the optimal EEMD is 0.2, 0.2062, and 0.0187, respectively. When the decomposition error is also fixed as 0.01, the $N$ values are 400, 425, and 4 accordingly. Table 10 illustrates the computational time and the orthogonality value. The IO values of the traditional EEMD and the improved EEMD are approximately equal to 4.5%, the decomposition accuracy is similar. In comparison, the IO value obtained by the optimal EEMD is one-fourth of the two former's. The result shows that the decomposition accuracy is improved. It is clear that the computational time of the optimal EEMD is approximately equal to 1/70 of the traditional

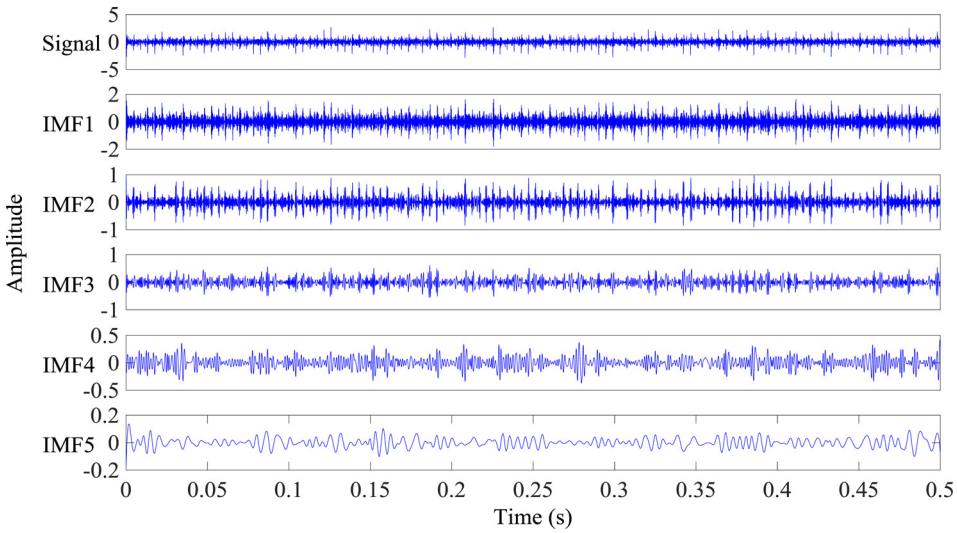


**Fig. 21 Result of vibration signals from defective bearing decomposed by the optimal EEMD**

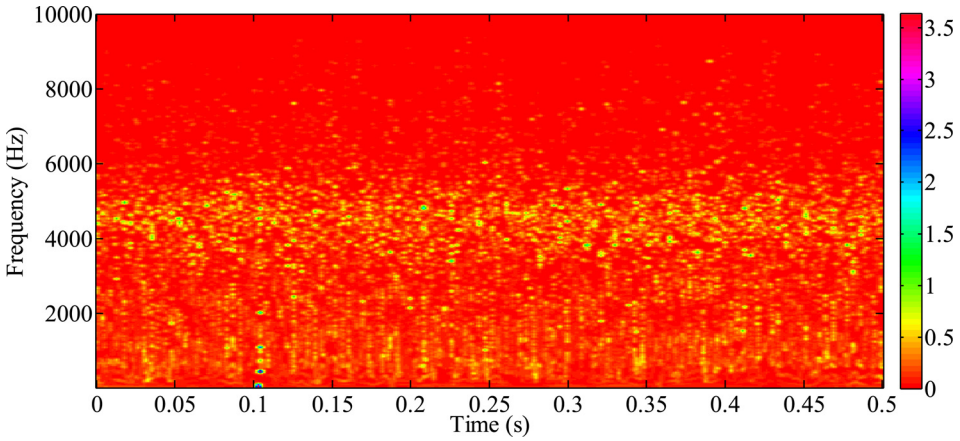


**Fig. 22 The HHT spectrum of defective bearing signals decomposed by the optimal EEMD**

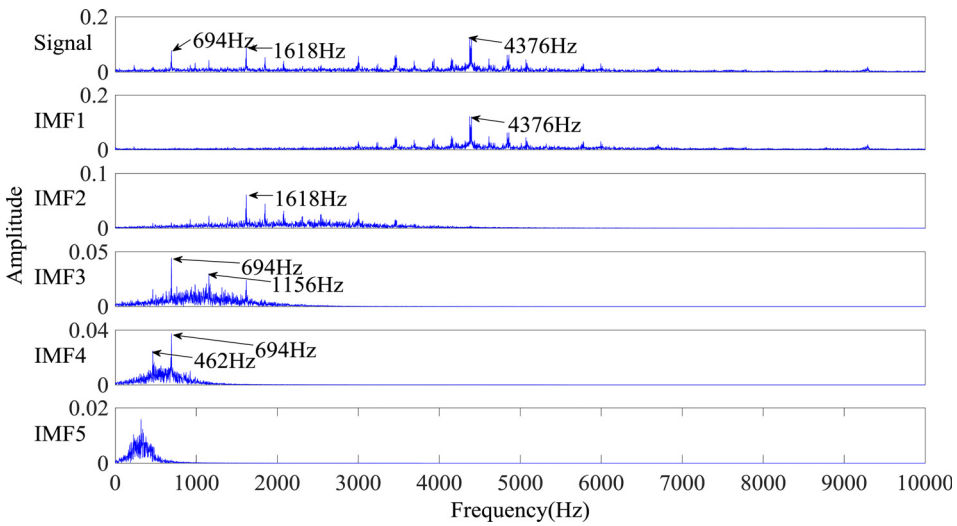


**Fig. 23 The frequency spectrum of defective bearing signals decomposed by the optimal EEMD**

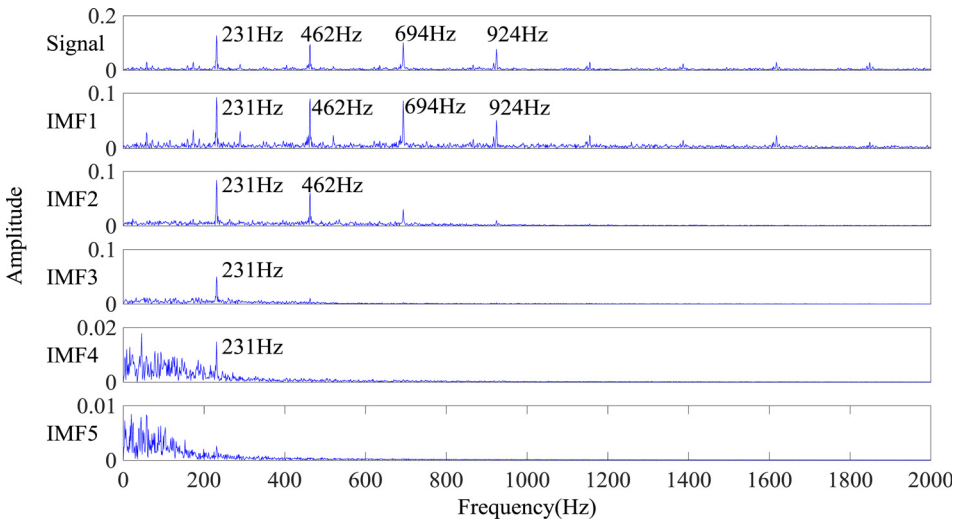


**Fig. 24 The envelope spectrum of defective bearing signals decomposed by the optimal EEMD**

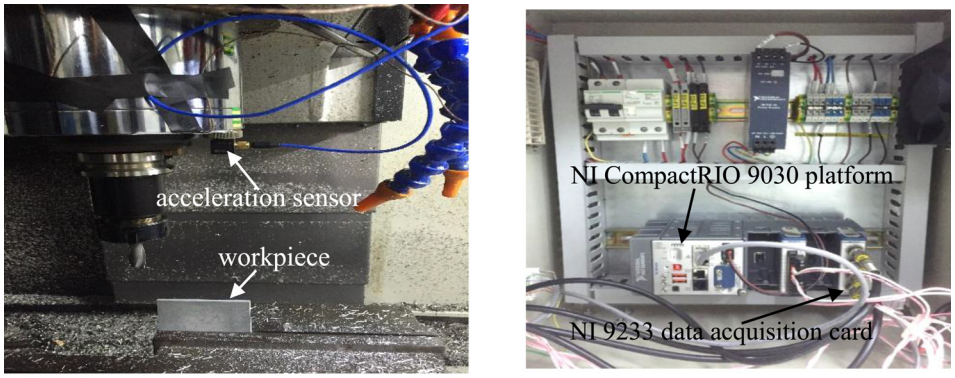


(*a*) (*b*)

**Fig. 25 The experimental setup**

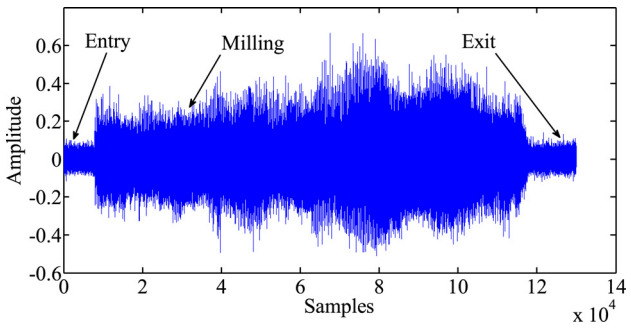


**Fig. 26 The original acceleration signal of one running sample**

**Table 11 Comparison of acceleration signals' analysis**

| Comparative item | Traditional EEMD [23] | Improved EEMD [34] | Optimal EEMD |
|---|---|---|---|
| $\alpha$ | 0.2 | 0.1901 | 0.0297 |
| $N$ | 400 | 361 | 9 |
| Computational time (s) | 466.67 | 387.64 | 7.37 |
| IO | 0.1127 | 0.1090 | 0.0066 |

EEMD's and 1/87 of the improved EEMD's, so the computational efficiency is greatly improved.

Figure 21 illustrates the first five IMFs of the decomposition result derived by the optimal EEMD for the vibration signal with bearing outer ring fault. Figures 22–24 are the HHT spectrum, the FFT spectrum, and the envelope spectrum, respectively. It can be seen that there are obviously periodic components. Compared to the inner ring defects, the impacts caused by the outer ring defects are stronger in the vibration signals. Therefore, detecting the outer race detect is relatively easy. According to the empirical formula, the characteristic frequency of the outer ring defect is 236.4 Hz as shown in Table 8. On the one hand, some special features are found in the FFT spectrum shown in Fig. 23, and these frequencies such as 462 Hz, 694 Hz, 1156 Hz, and 1618 Hz are clear. It also can be seen that these frequencies are twice, 3 times, 5 times, and 7 times of 231 Hz. On the other hand, the distinct regularity can be obtained from Fig. 23. Consequently, it can be concluded that the estimated characteristic frequency is 231 Hz. This frequency is close to the characteristic frequency. Hence, the optimal EEMD can effectively decompose the vibration signals from the bearing outer ring defect.

## 6 A Case Study

**6.1 Experiment Setup.** In order to investigate the effectiveness of the proposed method for vibration signal decomposition, a data set from a milling process is used. The machine is a three-axis vertical milling center VMC850E. The test workpieces are with thin-walled structure. The type of material is 2024T3 duralumin alloy. The sizes of the workpiece are 68 mm × 68 mm × 4 mm. LABVIEW is used for data acquisition. The data acquisition system

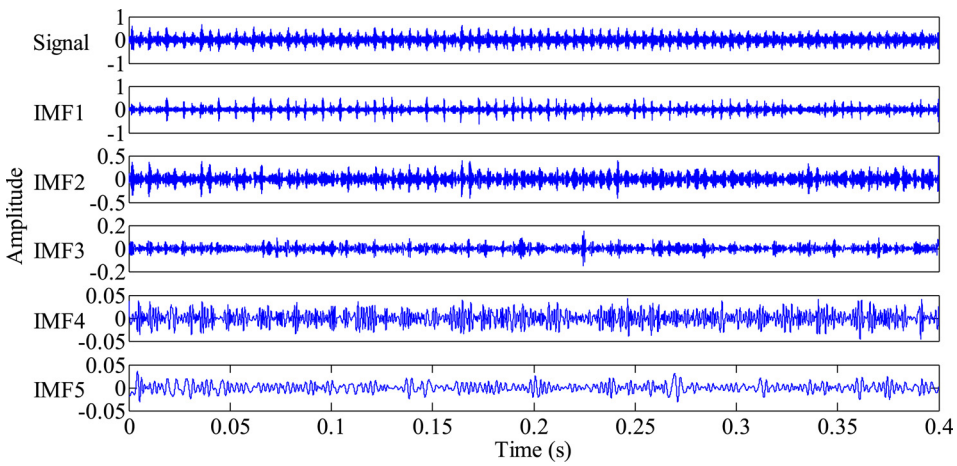


**Fig. 27 Results of acceleration signals decomposed by the optimal EEMD**

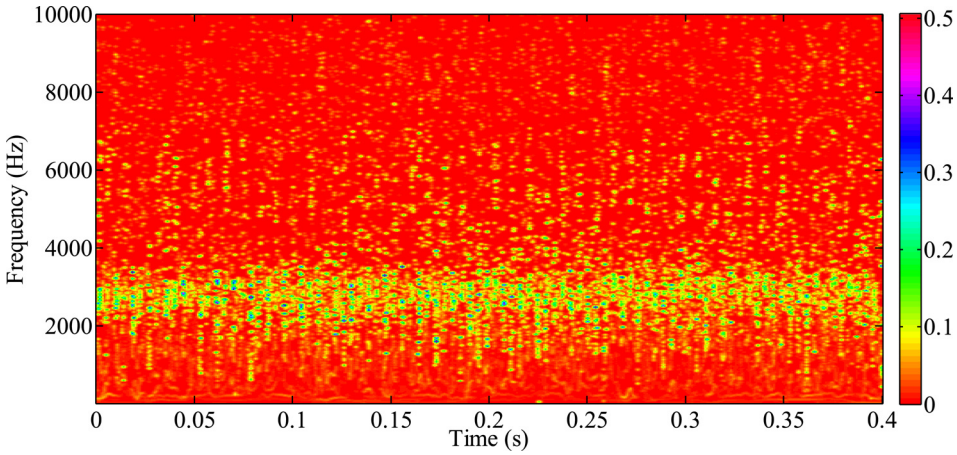


**Fig. 28 The HHT spectrum of acceleration signals decomposed by the optimal EEMD**

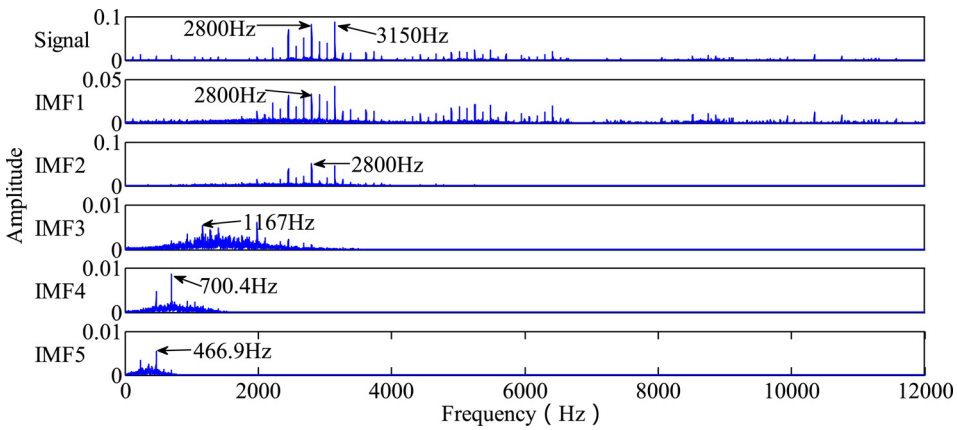


**Fig. 29 The frequency spectrum of acceleration signals decomposed by the optimal EEMD**

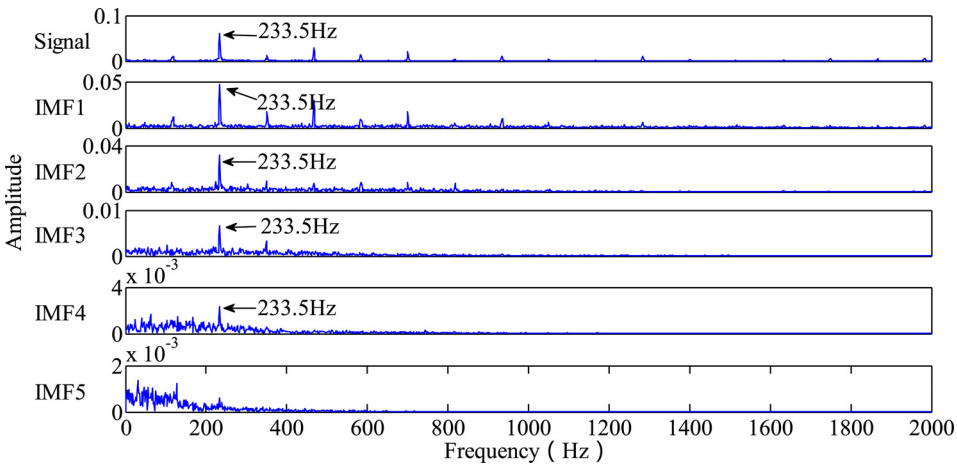


**Fig. 30 The envelope spectrum of acceleration signals decomposed by the optimal EEMD**

is composed of NI CompactRIO 9030, NI 9233, and a vibration sensor. The vibration sensor is a tri-axial acceleration sensor (Model 356A16). The data sampling rate is 25,000 Hz. Figure 25 is the experimental setup.

**6.2 Results and Analysis.** Figure 26 is one of the original signals from the acceleration sensor installed on a spindle bearing near the cutting tool. Approximately130,000 data points were collected for each milling run with the entry-milling-exit cutting procedure. About 10,000 samples were chosen to implement the decomposition experiment.

For the acceleration signals, the amplitude of added white noise $\alpha$ of the traditional EEMD, the improved EEMD, and the optimal EEMD is 0.2, 0.1901, and 0.0297, respectively. The decomposition error is set as 0.01, and the $N$ values are 400, 361, and 9 accordingly. The computational time and the orthogonality values

are shown in Table 11. The IO value of the traditional EEMD is close to the improved EEMD's. However, the IO value of the optimal EEMD is approximately equal to 1/17 of the two former's, which means that the decomposition accuracy is improved and the mode mixing is reduced. Obviously, the optimal EEMD is more effective compared to the two former methods.

Figure 27 is the first five IMFs of the decomposition result of acceleration signals derived by the optimal EEMD, where $N$ for each case is set as 100. Figures 28 and 29 are the HHT spectrum and the FFT spectrum, respectively. In Fig. 28, the energy density distribution is most concentrated near by the frequency of 3000 Hz. From Fig. 29, it can be seen that the frequency of 2800 Hz is the dominant frequency. The result of Fig. 29 is consistent with the result of Fig. 28. The distinct dominant frequency is 233.5 Hz from Fig. 30. At the same time, some special features are found in the FFT spectrum shown in Fig. 29, and these frequencies such as 466.9 Hz, 700.4 Hz, 1167 Hz, and 2800 Hz are clear. It also can be seen that these frequencies are appropriate 2 times, 3 times, 5 times, and 12 times of 233.5 Hz. In this experiment, the frequency 233.5 Hz is the motor rotation excitation frequency.

## 7 Conclusion

This paper presents an optimal EEMD method based on an adaptive algorithm and a multimode search algorithm, aiming at the optimization of the two critical parameters including the amplitude of added white noise and the number of ensemble trials to solve mode mixing problem. The simulation results demonstrate: (1) Given fixed $\alpha$ value, the decomposition error will decrease with the increase of the ensemble number accordingly. The influence of the change of the $N$ value on IO can be neglected. (2) Compared with the traditional EEMD and the improved EEMD, the proposed method achieves higher decomposition accuracy and faster computational efficiency. The two examples with bearing vibration signals and a case study also demonstrate that the optimal EEMD method can automatically obtain the appropriate EEMD parameters for the different scale signals. It can effectively implement the vibration signal decomposition without mode mixing.

This paper focuses on the use of the optimal EEMD method for signal decomposition, and some issues might be investigated in the future based on the proposed method. (1) Multiscale monitoring of mechanical systems. Many signals exhibit multiscale nature, and the characterization of multiscale patterns might improve the monitoring performances. Since the proposed optimal EEMD method for multiscale vibration signal decomposition have good performances, it can be further investigated and applied in monitoring of mechanical systems. (2) Fault diagnosis of mechanical systems. Different faults could have different effects on distinct scales of a signal. Through the proposed optimal EEMD method, a complex signal can be decomposed into a minimal number of physically relevant and interpretable patterns, and then the potential root causes might be identified. (3) Other mode search algorithms need to be investigated and used to enhance the proposed method.

## Acknowledgment

The authors greatly acknowledge the editor and the reviewers for their valuable comments and suggestions that have led to a substantial improvement of the paper. This work was supported by the Major Program of the National Natural Science Foundation of China (Grant No. 51535007), the National Natural Science Foundation of China (Grant No. 51275558), the National Key Science and Technology Research Program of China (Grant No. 2014ZX04015-021), and the State Key Lab of Mechanical System and Vibration program (Grant No. MSVZD201503).

## References

[1] Feng, Z., Liang, M., and Cu, F., 2013, "Recent Advances in Time-Frequency Analysis Methods for Machinery Fault Diagnosis: A Review With Application Examples," Mech. Syst. Signal Process., **38**(1), pp. 165–205.

[2] Roth, J. T., Djurdjanovic, D., Yang, X., Mears, L., and Kurfess, T., 2010, "Quality and Inspection of Machining Operations: Tool Condition Monitoring," ASME J. Manuf. Sci. Eng., **132**(4), p. 041015.

[3] Du, S., Lv, J., and Xi, L., 2012, "Degradation Process Prediction for Rotational Machinery Based on Hybrid Intelligent Model," Rob. Comput. Integr. Manuf., **28**(2), pp. 190–207.

[4] Lee, J., Wu, F. J., Zhao, W. Y., Ghaffari, M., Liao, L. X., and Siegel, D., 2014, "Prognostics and Health Management Design for Rotary Machinery Systems—Reviews, Methodology and Applications," Mech. Syst. Signal Process., **42**(1–2), pp. 314–334.

[5] Yang, Y., Dong, X. J., Peng, Z. K., Zhang, W. M., and Meng, G., 2015, "Vibration Signal Analysis Using Parameterized Time-Frequency Method for Features Extraction of Varying-Speed Rotary Machinery," J. Sound Vib., **335**(5), pp. 350–366.

[6] Luo, J. S., Yu, D. J., and Liang, M., 2012, "Application of Multi-Scale Chirplet Path Pursuit and Fractional Fourier Transform for Gear Fault Detection in Speed Up and Speed-Down Processes," J. Sound Vib., **331**(22), pp. 4971–4986.

[7] Lin, J., and Qu, L. S., 2000, "Feature Extraction Based on Morlet Wavelet and Its Application for Mechanical Fault Diagnosis," J. Sound Vib., **234**(1), pp. 135–148.

[8] Yang, Y., Zhang, W. M., Peng, Z. K., and Meng, G., 2013, "Multicomponent Signal Analysis Based on Polynomial Chirplet Transform," IEEE Trans. Ind. Electron., **60**(9), pp. 3948–3956.

[9] Peng, Z., Chu, F., and He, Y., 2002, "Vibration Signal Analysis and Feature Extraction Based on Reassigned Wavelet Scalogram," J. Sound Vib., **253**(5), pp. 1087–1100.

[10] Peng, F. Q., Yu, D. J., and Luo, J. S., 2011, "Sparse Signal Decomposition Method Based on Multi-Scale Chirplet and Its Application to the Fault Diagnosis of Gearboxes," Mech. Syst. Signal Process., **25**(2), pp. 549–557.

[11] Xu, C., Wang, C., and Liu, W., 2016, "Nonstationary Vibration Signal Analysis Using Wavelet-Based Time–Frequency Filter and Wigner–Ville Distribution," ASME J. Vib. Acoust., **138**(5), p. 051009.

[12] Peng, Z. K., and Chu, F. L., 2004, "Application of the Wavelet Transform in Machine Condition Monitoring and Fault Diagnostics: A Review With Bibliography," Mech. Syst. Signal Process., **18**(2), pp. 199–221.

[13] Peng, Z. K., Tse, P. W., and Chu, F. L., 2005, "An Improved Hilbert–Huang Transform and Its Application in Vibration Signal Analysis," J. Sound Vib., **286**(1–2), pp. 187–205.

[14] Yang, Y., Yu, D., and Cheng, J., 2006, "A Roller Bearing Fault Diagnosis Method Based on EMD Energy Entropy and ANN," J. Sound Vib., **294**(1–2), pp. 269–277.

[15] Hong, S., Wang, B., Li, G., and Hong, Q., 2014, "Performance Degradation Assessment for Bearing Based on Ensemble Empirical Mode Decomposition and Gaussian Mixture Model," ASME J. Vib. Acoust., **136**(6), p. 061006.

[16] Huang, N. E., Shen, Z., Long, S. R., Wu, M. L., Shih, H. H., Zheng, Q. N., Yen, N. C., Tung, C. C., and Liu, H. H., 1998, "The Empirical Mode Decomposition and the Hilbert Spectrum for Nonlinear and Non-Stationary Time Series Analysis," Proc.: Math., Phys. Eng. Sci., **454**(1971), pp. 903–995.

[17] Sun, Y., Zhuang, C., and Xiong, Z., 2015, "Transform Operator Pair Assisted Hilbert–Huang Transform for Signals With Instantaneous Frequency Intersections," ASME J. Vib. Acoust., **137**(6), p. 061016.

[18] Wang, K. S., and Heyns, P. S., 2011, "Application of Computed Order Tracking, Vold–Kalman Filtering and EMD in Rotating Machine Vibration," Mech. Syst. Signal Process., **25**(1), pp. 416–430.

[19] Lei, Y., Lin, J., He, Z., and Zuo, M. J., 2013, "A Review on Empirical Mode Decomposition in Fault Diagnosis of Rotating Machinery," Mech. Syst. Signal Process., **35**(1–2), pp. 108–126.

[20] Huang, N. E., Wu, M. L. C., Long, S. R., Shen, S. S. P., Qu, W. D., Gloersen, P., and Fan, K. L., 2003, "A Confidence Limit for the Empirical Mode Decomposition and Hilbert Spectral Analysis," Proc. R. Soc. London, A, **459**(2037), pp. 2317–2345.

[21] Deering, R., and Kaiser, J. E., 2005, "The Use of a Masking Signal to Improve Empirical Mode Decomposition," IEEE International Conference on Acoustics, Speech, and Signal Processing, 1–5: Speech Processing, Mar. 23, pp. 485–488.

[22] Grasso, M., and Colosimo, B. M., 2016, "An Automated Approach to Enhance Multiscale Signal Monitoring of Manufacturing Processes," ASME J. Manuf. Sci. Eng., **138**(5), p. 051003.

[23] Wu, Z., and Huang, N. E., 2009, "Ensemble Empirical Mode Decomposition: A Noise-Assisted Data Analysis Method," Adv. Adapt. Data Anal., Theory Appl., **1**(01), pp. 1–41.

[24] Peng, Y., 2006, "Empirical Model Decomposition Based Time-Frequency Analysis for the Effective Detection of Tool Breakage," ASME J. Manuf. Sci. Eng., **128**(1), pp. 154–166.

[25] Guo, W., and Tse, P. W., 2013, "A Novel Signal Compression Method Based on Optimal Ensemble Empirical Mode Decomposition for Bearing Vibration Signals," J. Sound Vib., **332**(2), pp. 423–441.

[26] Guo, W., and Tse, P. W., 2010, "Enhancing the Ability of Ensemble Empirical Mode Decomposition in Machine Fault Diagnosis," Prognostics & Health Management Conference, Jan. 12–14.

[27] Amarnath, M., and Krishna, I. R. P., 2013, "Detection and Diagnosis of Surface Wear Failure in a Spur Geared System Using EEMD Based Vibration Signal Analysis," Tribol. Int., **61**, pp. 224–234.

[28] Feng, Z. P., Liang, M., Zhang, Y., and Hou, S. M., 2012, "Fault Diagnosis for Wind Turbine Planetary Gearboxes Via Demodulation Analysis Based on Ensemble Empirical Mode Decomposition and Energy Separation," Renewable Energy, **47**, pp. 112–126.

[29] Caesarendra, W., Kosasih, P. B., Tieu, A. K., Moodie, C. A. S., and Choi, B. K., 2013, "Condition Monitoring of Naturally Damaged Slow Speed Slewing Bearing Based on Ensemble Empirical Mode Decomposition," J. Mech. Sci. Technol., **27**(8), pp. 2253–2262.
[30] Tabrizi, A., Garibaldi, L., Fasana, A., and Marchesiello, S., 2015, "Early Damage Detection of Roller Bearings Using Wavelet Packet Decomposition, Ensemble Empirical Mode Decomposition and Support Vector Machine," Meccanica, **50**(3), pp. 865–874.
[31] Georgoulas, G., Tsoumas, I. P., Antonino-Daviu, J. A., Climente-Alarcon, V., Stylios, C. D., Mitronikas, E. D., and Safacas, A. N., 2014, "Automatic Pattern Identification Based on the Complex Empirical Mode Decomposition of the Startup Current for the Diagnosis of Rotor Asymmetries in Asynchronous Machines," IEEE Trans. Ind. Electron., **61**(9), pp. 4937–4946.
[32] Yan, R., and Gao, R. X., 2008, "Rotary Machine Health Diagnosis Based on Empirical Mode Decomposition," ASME J. Vib. Acoust., **130**(2), p. 021007.
[33] Feng, Z., Zuo, M. J., Hao, R., Chu, F., and Lee, J., 2013, "Ensemble Empirical Mode Decomposition-Based Teager Energy Spectrum for Bearing Fault Diagnosis," ASME J. Vib. Acoust., **135**(3), p. 031013.
[34] Chen, L., Zi, Y. Y., He, Z. J., Lei, Y. G., and Tang, G. S., 2014, "Rotating Machinery Fault Detection Based on Improved Ensemble Empirical Mode Decomposition," Adv. Adapt. Data Anal., **6**(2–3), p. 1450006.
[35] Zhang, J. A., Yan, R. Q., Gao, R. X., and Feng, Z. H., 2010, "Performance Enhancement of Ensemble Empirical Mode Decomposition," Mech. Syst. Signal Process., **24**(7), pp. 2104–2123.
[36] Yeh, J.-R., Shieh, J.-S., and Huang, N. E., 2010, "Complementary Ensemble Empirical Mode Decomposition: A Novel Noise Enhanced Data Analysis Method," Adv. Adapt. Data Anal., **2**(2), pp. 135–156.
[37] Bekka, R. E. H., and Berrouche, Y., 2013, "Improvement of Ensemble Empirical Mode Decomposition by Over-Sampling," Adv. Adapt. Data Anal., **5**(3), p. 1350012.
[38] Zheng, J. D., Cheng, J. S., and Yang, Y., 2014, "Partly Ensemble Empirical Mode Decomposition: An Improved Noise-Assisted Method for Eliminating Mode Mixing," Signal Process., **96**, pp. 362–374.
[39] Xue, X. M., Zhou, J. Z., Xu, Y. H., Zhu, W. L., and Li, C. S., 2015, "An Adaptively Fast Ensemble Empirical Mode Decomposition Method and Its Applications to Rolling Element Bearing Fault Diagnosis," Mech. Syst. Signal Process., **62–63**, pp. 444–459.
[40] Hooke, R., and Jeeves, T. A., 1961, "Direct Search Solution of Numerical and Statistical Problems," J. ACM, **8**(2), pp. 212–229.
[41] CWRU, 2015, "Bearing Data Center," Case Western University, Cleveland, OH.
[42] NASAARC, 2015, "IMS Bearings Data Set," NASA Ames Research Center, Moffett Field, CA.